Evaporation and fission decay of ^{158}Er composite nuclei within the statistical model

A. Di Nitto,[1,2,*] E. Vardaci,[1,2] G. La Rana,[1,2] P. N. Nadtochy,[2,3] A. Boiano,[2] M. Cinausero,[4] G. Prete,[4] N. Gelli,[5] E. M. Kozulin,[6] G. N. Knyazheva,[6] A. Ordine,[2] F. Davide,[1] C. Parascandolo,[2] D. Pierroutsakou,[2] and A. Pulcini[1,2]

[1]*Dipartimento di Fisica "E. Pancini," Universitá degli Studi di Napoli "Federico II," Napoli, Italy*

[2]*Istituto Nazionale di Fisica Nucleare, Sezione di Napoli, Napoli, Italy*

[3]*Omsk State Technical University, Mira prospekt 11, 644050 Omsk, Russia*

[4]*Istituto Nazionale di Fisica Nucleare, Laboratori Nazionali di Legnaro, Legnaro (Padova), Italy*

[5]*Istituto Nazionale di Fisica Nucleare, Sezione di Firenze, Firenze, Italy*

[6]*Flerov Laboratory of Nuclear Reactions, Joint Institute for Nuclear Research, Dubna, Russia*

(Received 27 February 2020; revised 18 May 2020; accepted 16 July 2020; published 24 August 2020)

Light charged particles emitted by the compound nucleus ^{158}Er produced in the reaction ^{32}S (180 MeV) + ^{126}Te, at the excitation energy $E_x = 92$ MeV, have been measured at Laboratori Nazionali di Legnaro in coincidence with fission fragments and evaporation residues. The 4π detector array 8πLP coupled to a system of parallel-plate avalanche counters to detect evaporation residues has been used. Data have been analyzed in the framework of the statistical model of evaporation with the code PACE2_N11. This enlarged version of the code PACE2 has been used to reproduce the large set of observables measured in the fusion-evaporation and fusion-fission channels along with experimental prescission neutron multiplicity and fission cross section taken from literature. It is found that the simultaneous reproduction of the prescission neutron, proton, and α-particle multiplicities can be obtained with zero fission delay without dynamical effects. However, the same set of model input parameters does not allow us to reproduce proton and α-particle multiplicities in the evaporation channel. Extensive calculations, with different sets of parameters, show the limits of the statistical model in reproducing the whole set of data. This work evidences the importance of measuring a large set of observables in order to obtain a reliable description of the decay of the compound nucleus, and in particular of the fission process.

DOI: 10.1103/PhysRevC.102.024624

I. INTRODUCTION

After 80 years [1,2], the fission process still is a frontier of modern nuclear physics. The large effort dedicated to this topic since 1939 has uncovered many peculiarities of the phenomenon, but a definitive description is still missing [3,4].

The reason for this is the large complexity of the process. This complexity originates in the interplay between the collective (macroscopic) and single-particle (microscopic) degrees of freedom in the nucleus. The specifics of the decay of the compound nucleus are sensitive to this interplay. For instance, the dynamical evolution of the nuclear shapes determines the fission yield as well as the competition with the evaporation channel. Consequently, this interplay affects the production rates of exotic nuclei at isotope separator on-line facilities as well as the production of superheavy elements in fusion-evaporation reactions.

New properties of the fission process have been outlined by investigating nuclei located far from the stability line. Not only fusion reactions [5,6] but also a large variety of different nuclear reactions have been used to populate fissioning nuclei at very low and very high excitation energies, in particular, few-nucleon direct transfer [7,8] and spallation reactions [9]. In heavier mass regions, the quasifission (QF) process appears [10]. QF consists of the decay of a dinuclear system, formed by the capture of projectile and target nuclei, without forming a compound nucleus (CN). QF is the main antagonist to the complete fusion when the atomic numbers of the projectile Z_P and the target Z_T lead to $Z_P Z_T > 1600$. The competition between complete fusion and QF is roughly a decreasing monotonic function with increasing $Z_1 Z_2$, but also is influenced by characteristic properties of the colliding nuclei [11]. Under the influence of proton and neutron shell closures ($Z = 82$; $N = 82$, 126) and shape orientation effects, QF enhances the production of nuclei with masses around 208 u and reduces the chances of forming superheavy nuclei [10,12–14]. At high values of the initial orbital angular momentum l_i, fast fission can also occur. Fast fission consists of the disintegration into two fragments of the intermediate mononucleus that survives against QF. Both QF and fast-fission processes bypass the stage of the CN formation. The difference between the two processes is in their dependence on the orbital angular momentum: QF can takes place at all orbital angular momenta, whereas fast fission is possible only at $l_i > l_f$, where l_f is the angular momentum value at which the fission barrier of the compound nucleus disappears [15].

In this work, we present a study of the fission and evaporation decay channels of an intermediate-mass compound nucleus produced in a fusion reaction induced by heavy ions.

*Corresponding author: dinitto@na.infn.it

It is well established that fusion-fission (FF) is a slow process dominated by nuclear viscosity [16,17]. A very striking experimental evidence of such behavior is the excess of prescission light particles (LP) with respect to the predictions of the statistical model (SM) and its dependence on the excitation energy [18–20]. Phenomenological studies based on the SM predictions were carried out with the aim to estimate the fission timescale, and, in some cases, to obtain information on the dissipation mechanism [21–23]. Estimates given by different authors predict wide ranges for the fission timescale and nuclear viscosity strength (see reviews [24–26] and references therein). The main reason of this wide range can be related to the different probes used. In recent decades [27,28], and again very recently [29,30], besides the fission timescale, other aspects related to fission dynamics (i.e., nuclear deformation at different stages, dependence of the dissipation mechanism from temperature or deformation) have been extracted by considering a limited number of observables measured in the fission channel. Consequently, stringent constraints are not imposed to SM parameters. In addition, this kind of approach is founded on the reliability of the SM to reproduce the observables in the evaporation residue (ER) channel. However, this reliability has not yet been fully explored. The search for a strategy to identify the physical ingredients that drive the fission process and to uniquely determine the SM parameters appears to be the main issue. The ultimate goal is to attain a consistent picture of the fission process.

In our approach, we start by noting that the dynamics of the fission process is expected to affect the ER channel, because of the fission hindrance due to nuclear viscosity. For this reason, the study of the evaporation residues channel can play a very important role. The importance of this approach was already pointed out in previous works reporting on the investigation of the reaction $^{32}\mathrm{S} + {}^{100}\mathrm{Mo}$ at 200 MeV [31,32]. Systems of intermediate fissility represent a suitable environment to connect FF and ER channels. They are characterized by ER and FF cross sections of the same order of magnitude and large emission probability of light charged particles (LCPs). Observables related to LCPs provide fundamental indications for constraining SM leading parameters because LCPs are very sensitive to the nuclear charge distribution [33].

In order to fully benchmark existing models, in our opinion it is crucial to enlarge the data set available for reactions of interest. Here, we report on the observables measured in the evaporation and fission decays of compound nucleus $^{158}\mathrm{Er}$ at excitation energy of 92 MeV produced in the 180 MeV $^{32}\mathrm{S} + {}^{126}\mathrm{Te}$ reaction. For this system, we measured the LCP multiplicities in the fission and evaporation channels, as well as energy-integrated differential multiplicities and energy spectra of the evaporative LCPs. On this large data set, extended further with the prescission neutron multiplicity [34] and the fusion-fission cross section [35] found in the literature, we propose here a detailed SM analysis of the fission and evaporation decays. We test different physical ingredients of the model. The addition of the prescission neutron multiplicity to our set of data, neutron emission in competition with the LCP emission, represents a further constraint to explore the existing ambiguities on the fusion-fission decay [22,36].

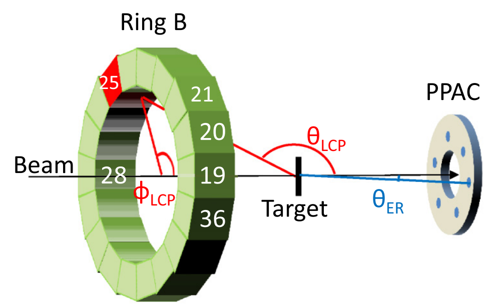

FIG. 1. Schematic of a coincident event: the LCP is detected by the Ball telescope number 25, and the ER by a sector of the annular parallel-plate avalanche counter (PPAC). The line connecting the target with the center of the PPAC sector at θ_{ER} and the beam direction define the reaction plane. The direction of LCPs impinging on a Ball telescope is defined by the polar angle θ_{LCP} and azimuthal angle ϕ_{LCP}. Ring B (at $\theta_{\mathrm{LCP}} = 137^{\circ}$ with respect to the beam direction) is shown. It is made of 18 identical bitelescopes mounted at same polar angle and spanning all the possible azimuthal angles. There are seven rings in 8πLP, named from A to G, from backward to forward directions, respectively, each containing a replica of the same bitelescope.

The limits of the SM approach were already highlighted in previous works using an extended data set for another reaction [31,37]. However, there is still substantial room for improving our knowledge of the compound nucleus decay and to confirm or reject our previous findings.

The paper is organized as it follows. Details of the experimental setup are presented in Sec. II. Experimental data on the reaction $^{32}\mathrm{S} + {}^{126}\mathrm{Te}$ at 180 MeV are shown in Sec. III. In Sec. IV, we discuss some aspects relevant for this study with the SM code PACE2_N11. Section V is dedicated to the interpretation of the experimental data by means of comparisons with the SM calculations. In Sec. VI, we draw our conclusions.

II. EXPERIMENTAL SETUP

The experiment was performed at the XTU-Tandem accelerator of Laboratori Nazionali di Legnaro (Italy). A pulsed beam of $^{32}\mathrm{S}$ ions with an intensity of about 0.1–0.3 particle nA at 180 MeV was used to bombard a self-supporting $^{126}\mathrm{Te}$ target 400 $\mu\mathrm{g/cm}^2$ thick. A beam burst with period of 800 ns and duration of about 3 ns was used.

We used the Ball sector 8πLP apparatus [38] to detect LCPs in coincidence with fission fragments and evaporation residues.

The Ball apparatus is a sphere of 126 bitelescopes arranged in seven rings. It has a diameter of 30 cm and covers the polar angles from 34° to 165° with respect to the beam direction. The schematic draw of one backward ring is shown in Fig. 1. Each ring contains 18 identical bitelescopes and covers a polar angular opening of about 17°. In this geometry, the 18 detectors of a ring have the same average polar angle and all together cover the azimuthal angle from 0 to 2π. As a whole, the Ball apparatus covers a solid angle of about 80% of 4π. Each bitelescope is made of a first stage (ΔE) of a 300-μm-thick Si detector followed by a second stage

(E) of 5-mm-thick CsI(Tl) with photodiode readout. Fission fragments and slower LCPs stopped in the first stage of the telescopes are separated by using a pulse shape discrimination (PSD) technique [39]. In particular, this technique allows also the charge identification of lighter particles ($Z \leqslant 3$). For LCPs passing through the first stage, it is also possible to identify isotopes by using the ΔE-E technique.

Heavy fragments from two-body reactions were detected in double-coincidence mode in the bitelescopes of the most forward rings of the Ball apparatus, which cover the angles from 34° to 70° (rings F and G). Because these fragments do not cross the first stage of the telescope, the PSD technique was used to discriminate them against the LCP stopping in the ΔE detector of the same bitelescope. Further details are given in Ref. [31].

To detect evaporation residues, 8πLP is equipped with an annular PPAC system divided into six independent sectors mounted 62 cm from the target (Fig. 1). The system consists of two PPACs, a front and a rear one, coaxially mounted and separated by a polypropylene foil 15 μm thick in between. The foil is chosen to be thick enough to stop the ERs passing through the front PPAC and sufficiently thin that the faster particles, from fission fragment up to elastically scattered beam ions, can hit the rear PPAC. With this coaxial configuration, the rear PPAC signals are used to efficiently reject the ions different than evaporation residues. From the time-of-flight spectra (obtained as the time difference between the beam pulse radio frequency signal and that from the front PPAC in anticoincidence with the rear PPAC), the identification of ERs is achieved.

In order to define, for this experiment, a narrow angular detection windows for the ERs, a mask with six holes of 1-cm radius was mounted in front of the PPAC system. In this way, we could define six independent (trigger) detectors, each one centered at 4° with respect to the beam direction. The symmetrical positioning of the PPAC is very useful because one can benefit from the spherical symmetry of the Ball apparatus. Each direction of the six PPACs defines, along with the beam direction, a reaction plane in the ER channel. Each reaction plane selects a direction of the spin of the compound nucleus (orthogonal to the reaction plane) with some misalignment owing to particle evaporation (considered later in the simulations). For each reaction plane (namely, for each spin direction), extended in-plane and out-of-plane distributions can be measured by choosing the detectors of a ring spanning the azimuthal angle $\phi_{\rm LCP}$ from 0 to 2π, and whose polar angle $\theta_{\rm LCP}$ is fixed by the chosen ring (Fig. 1). In this way, it is possible to highlight the effect of the spin on the angular distribution, and the different kinematical kick and event rates when the LCP is observed on the opposite side of the PPAC (higher rate) or on the same side (lower rate) with respect to the beam. Furthermore, the coincidence events between the Ball apparatus and each PPAC can be summed correspondingly to improve the statistics.

The acquisition system is based on the Fast Intercrate Readout [40] and Vme Interfaced to Pci Easy Readout System [41–45] data acquisition systems running a Versa Module Europa front-end with commercial Time-to-Digital Converter and Analog-to-Digital Converter modules. Data were collected with the following conditions in OR mode: (a) coincidences between a PPAC sector and a Ball telescope (to select the LCP's from fusion-evaporation reactions); (b) events detected by a PPAC sector (to detect ER events in single mode); (c) twofold events in the F and G rings telescopes (for fission fragments in single mode); and (d) threefold events between bitelescopes of the F or G rings and any other bitelescope of the Ball apparatus (to select LCPs in coincidence with fission fragments). Thus, by performing single and coincidence measurements in the same run, systematic errors are strongly suppressed. Data sorting and analysis were handled by the software package VISM [46].

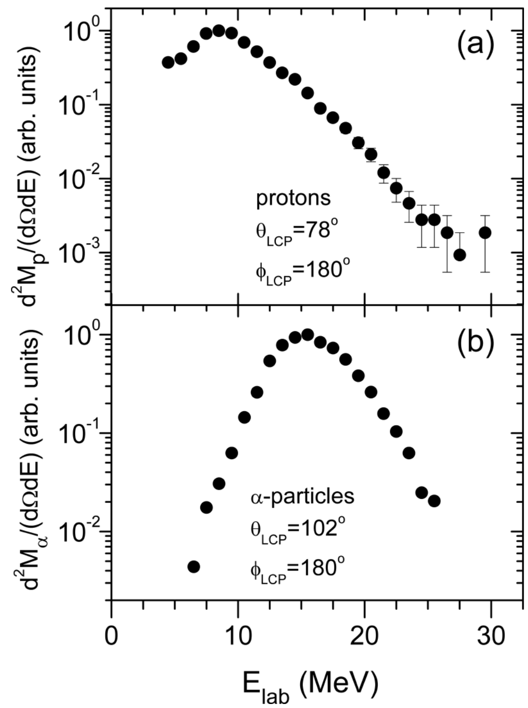

FIG. 2. (a) Proton and (b) α-particle energy spectra measured with two 8πLP Ball telescopes in coincidence with ERs in the PPAC. The spectra are normalized to 1 at the maximum.

III. EXPERIMENTAL DATA

A. LCPs emission in the ER channel

Multiplicities, energy spectra, and angular distributions of LCPs in the FF and ER channels were extracted from raw data after proper energy calibration and particle identification. A detailed description of the whole process can be found in Refs. [31,47,48].

An example of proton and α-particle energy spectra measured with Ball telescopes at different position ($\theta_{\rm LCP}$ and $\phi_{\rm LCP}$) in coincidence with ERs in one of the PPAC sectors is shown in Fig. 2.

The energy-integrated differential multiplicities (DMs) for protons and α particles in the ER channel are shown in Fig. 3 as a function of the Ball detector number. The specific enumeration given to each telescope, in connection with the corresponding azimuthal angles spanning from 0 to 2π, gives

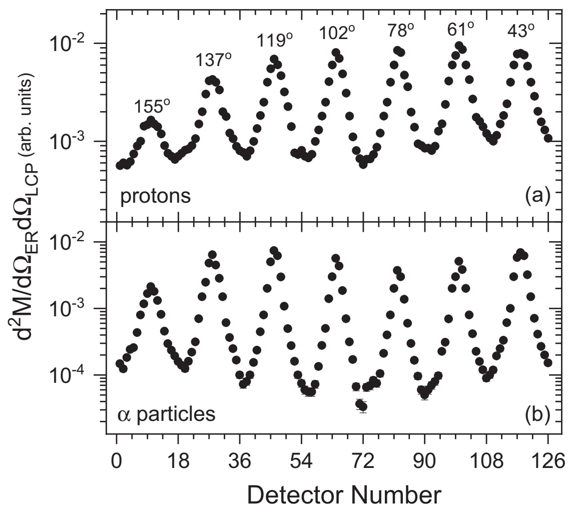

FIG. 3. (a) Proton and (b) α-particle energy-integrated differential multiplicities measured in coincidence with ERs identified in the PPAC system as function of the 8πLP Ball telescopes number. The polar angles θ_{LCP} corresponding to the rings of the Ball are reported.

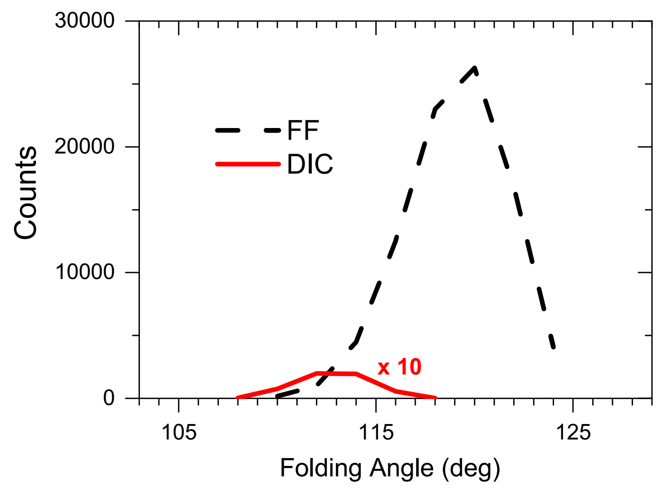

FIG. 4. Folding angle distributions of binary fragments from fusion-fission channel (FF, dashed black line) and deep inelastic collisions (DIC, solid red line). Viola total kinetic energy systematics [50] and constraints of detector geometry in ring F ($\langle\theta_{\mathrm{lab}}\rangle = 61^\circ$, $\Delta\theta_{\mathrm{lab}} = 17^\circ$) were employed.

rise to characteristic peaks. They are due to a combined effect of kinematics and spin of the composite system (orthogonal to the reaction plane). The maxima correspond to the events where ERs and LCPs are in plane and on the opposite sides of the beam direction; the minima occur when ERs and LCPs are in plane and on the same side of the beam direction. In order to reduce statistical fluctuations, the data collected using different PPAC-LCP telescope combinations were merged together when they correspond to the same angle between the PPAC detector and the telescope detector. The LCP multiplicities were extracted taking into account the detection efficiency of our detection system. Details of the procedure are in Ref. [31]. The obtained multiplicitites are reported in Table I.

B. LCP's emission in the fission channel

For the reaction under study, we expect binary fragments from fusion-fission and from deep inelastic collisions (DIC). In principle, fragments from DIC could pollute the mass distribution of the fragments from FF and consequently the FF-LCP coincidences. However, the mass and energy distributions of the fission fragments are expected to be symmetric, whereas binary products from DIC are characterized by a mass distribution peaked around the projectile and the target masses. The energy distribution is therefore also asymmetric.

TABLE I. Experimental proton and α-particle multiplicities in the ER and prescission channels for the reaction 180-MeV $^{32}\mathrm{S} + {}^{126}\mathrm{Te}$. The reported values have been estimated by taking into account the efficiency of the detection setup.

	ER	Prescission
M_p	0.375(0.075)	0.034(0.007)
M_α	0.234(0.047)	0.020(0.004)

This means, from momentum conservation, that fragments from FF and from DIC channels have folding angle distributions with different averages and widths. The average folding angle is defined as $\langle\theta_{1,\mathrm{lab}} + \theta_{2,\mathrm{lab}}\rangle$, where $\theta_{1,\mathrm{lab}}$ and $\theta_{2,\mathrm{lab}}$ are the angles of the two fragments in the laboratory frame. The folding angle distributions were computed, by a Monte Carlo method, with the code GANES [49] and are shown in Fig. 4. We employed the Viola systematics for the total kinetic energy [50] of the two fragments in the center-of-mass frame and constrained the detection geometry to the laboratory angles corresponding to the ring F. The fold distribution of the DIC fragments extends partially under the distribution of the fission fragments, but its contribution is negligible. Therefore, fission fragments can be discriminated against DIC fragments by selecting coincidences between fragments in two opponent detectors of ring F.

Laboratory energy spectra of protons and α particles in the fission channel were obtained from triple coincidence among any telescopes and two fission fragments in two opposite telescopes ($\Delta\phi_{\mathrm{FF}} = 180^\circ$) in ring F. To reduce fluctuations, a summing procedure was adopted as well. Each LCP spectrum corresponds to an angular configuration (α, β) with respect to the reaction plane (defined by the two fission fragment trajectories), where α and β are the in-plane and out-of-plane angles, respectively. Thanks to the symmetrical arrangement of the Ball telescopes, by rotating around the beam axis it is possible to obtain nine reaction planes, and, consequently, there are nine triple correlations corresponding to the same in-plane and out-of-plane angles. The corresponding spectra have been summed together.

We performed a multisources analysis of particle spectra to extract the pre- and postscission angle-integrated multiplicities. We used a well-established procedure that employs the code GANES [49,51–53] and that takes advantage of the different kinematics of the three emission sources (composite nucleus prior to scission and the two fully accelerated fission fragments). In this procedure, proton and α-particle evaporative spectra are computed separately for each emitting source in the experimental detection conditions within the window of angular momentum associated to FF. In our case, the window is 68–76$\hbar$ as extracted from the measured channel cross section σ_{FF} and the Bass prediction of the fusion cross section σ_{fus}. The calculated spectra, for each emitting source, are afterward normalized to the experimental spectra at the angles where their contribution is kinematically separated from those of the other sources. The normalization at the appropriate angles fixes the intensity of the contribution of each source at all the other angles, as imposed by the angular distributions from GANES. Accordingly, an iterative procedure developed to optimize the normalization of the three components to the data was applied (see description in Ref. [31]). Once the bulk of the experimental spectra is reasonably well reproduced over a wide angular coverage of the detector array, the integration by GANES over 4π of the resulting angular distributions was used to get the proton and α-particle prescission multiplicities reported in Table I.

IV. MODEL

In this section, we highlight some features of the SM code we used to attempt a description of the large set of data gathered for the reaction ^{32}S (180 MeV) + ^{126}Te. It is known that the SM approach to the description of the fission dynamics allows a fair description of observables in the fission channel [18–21,27,28,54,55], but we also claim that it shows several limits [31,37] when it is applied to a larger set of data. It is not uncommon that different sets of input parameters can result in equally good fits to a limited set of data within the same model [21,56]. Furthermore, the SM provides a description of the evolution of the compound nucleus en route to fission at variance with the picture offered by dynamical models [57]. Even though the dynamical approach seems, at first glance, more realistic, the dichotomy between the statistical and dynamical approaches is still far from being solved. In our opinion, a detailed statistical model analysis turns out to be essential and complementary to the dynamical model one.

Several computer codes implement the statistical model to predict ER and FF reactions observables [19,58–60]. We have traditionally worked with the well-known computer code PACE2 [61]. PACE2 simulates the multistep de-excitation of the compound nucleus both through fission and light particle evaporation (n, p, α). Light particle evaporation is implemented according to the Hauser-Feshbach formulation and the fission probability is calculated by using the transition-state model. Fission barriers are computed with the finite-range liquid drop model (FRLDM) [62]. The competition between the fission and evaporation modes is treated with a Monte Carlo approach.

We have constantly and extensively updated this code and to distinguish it from the original version we named the new version PACE2_N11 [31]. The original code was modified to implement different prescriptions for leading ingredients of the light particle emissions (transmission coefficients, level density parameters, and yrast lines). Other than this, the code now offers to modify the fission-evaporation competitions by using the ratio a_f/a_ν and to include a fission delay time τ_d by means of a simple step function. The parameter a_ν is the Fermi gas level density parameter for particle evaporation and a_f is the level density parameter for fission. For values of $a_f/a_\nu > 1$, the competition favors fission decay. The fission delay time τ_d is a parameter that turns off the fission probability and defines for how long the fission is artificially suppressed to favor particle evaporation. It is also called the presaddle delay, namely, the characteristic time that the composite system spends inside the barrier and only particle evaporation is allowed. The effect of increasing values of the parameter τ_d is an increasingly larger multiplicities of light particles before fission saddle point (larger prescission multiplicities). The parameters a_f/a_ν and τ_d are usually tuned to reproduce the FF decay channel observables (see, for instance, Refs. [18,19,34,35]).

The advantage coming from the use of a Monte Carlo code, such as PACE2_N11, is the possibility to generate an event output file. The file includes information on the energy and angular distributions of light particles and evaporation residues for each decay cascade in the center-of-mass or laboratory frame. Afterward, the event file can be filtered to take into account the geometrical efficiency of the detection setup and experimental conditions (i.e., energy threshold of the detectors). Hence, the observables obtained as a result of this procedure can be directly compared with the experimental data.

The dependence of our calculations on a_f/a_ν and τ_d are only briefly discussed due to the limited impact on our conclusions as it was already found in similar reactions on intermediate mass systems [33,57]. The following discussion is aimed instead at investigating the reliability of the SM in reproducing a large set of observables in the ER channel. This is a crucial point because such a reliability is a prerequisite to the application of the SM to the study of fission dynamics. This comparison between data in the ER channel and the predictions of the SM constitutes also a mean to identify additional observables able to provide further constraints to the models, statistical or dynamical, aimed at describing fission dynamics.

V. RESULTS AND DISCUSSION

Extensive SM calculations have been carried out to reproduce the whole set of data available by using different models for the three main ingredients of the SM: transmission coefficients, yrast lines, and level density parameter "little a." Table II shows the combinations that better reproduce the experimental data considering the following choices of models: (i) transmission coefficients (TC) from optical model (OM) [63–65] and from fusion systematics (FS) [66] with different barrier curvatures $\hbar\omega_n$, $\hbar\omega_p$, and $\hbar\omega_\alpha$, for neutrons, protons, and α particles, respectively; (ii) yrast lines (YL) calculated with parameters from the rotating liquid drop model (LDM) [15] and assuming the rigid sphere (RS) approximation for the CN with $r_0 = 1.21$–1.65 fm; (iii) level density parameter "little a" ranging from $A/6$ to $A/12$.

TABLE II. SM parameters adopted in the PACE simulations for the $^{32}S + ^{126}Te$ reaction.

Combination	a	TC	$\hbar\omega_n$, $\hbar\omega_p$, $\hbar\omega_\alpha$ (MeV)	YL	r_0 (fm)
a	A/6	FS	4.0, 4.0, 3.5	RS	1.21
b	A/6	OM		RS	1.21
c	A/6	FS	4.0, 4.0, 3.5	LDM	
d	A/12	FS	4.0, 4.0, 3.5	RS	1.21
e	A/12	OM		LDM	
f	A/7	FS	9.5, 4.0, 0.5	RS	1.65

Among the many calculations performed, only the six most meaningful combinations of models are presented. With reference to Table II, the combination (a) was considered because it better reproduces the fusion-evaporation and fusion-fission experimental data of the reaction $^{32}S + ^{100}Mo$ using different simulation codes [32]. Calculations with combinations (b), (c), and (d) evidence the influence of the used prescriptions on the observables: Optical model versus fusion systematics; rigid sphere versus liquid drop model, and level density parameter $a = A/6$ versus $a = A/12$.

Combination (e) provides the largest reduction of neutron multiplicities, so therefore it can be considered as the one requiring the largest fission delay according to the neutron-clock approach [18]. Finally, combination (f) is aimed at testing the influence of the FS-TC barrier curvature values and moment of inertia on the level density with the aim to explore the capability of the model to reproduce the LP multiplicities without any fission delay, as discussed in the next. In particular, this combination assumes a larger volume of emitting nuclei (accomplished by assuming the compound nucleus as a rigid sphere, whose radius parameter is $r_0 = 1.65$ fm) and FS-TC with $\hbar\omega_n = 9.5\,MeV$, $\hbar\omega_p = 4.0$ MeV, and $\hbar\omega_\alpha = 0.5\,$MeV.

We now proceed by showing the effects of the different combinations of models on the observed data. We focus our attention on the ER channel as our strategy is to verify if the SM can reproduce the observed data before applying it also to the FF channel data. We also consider the excitation function of σ_{FF} as this is correlated to the ER cross section (σ_{ER}) by the maximum entrance channel orbital angular momentum.

A. Fusion-fission excitation function

We show in Fig. 5 σ_{FF} calculations of PACE2_N11, using combinations (a) and (e), superimposed on the data. All combinations in Table II allow us to reproduce reasonably well the σ_{FF} behavior below $E_{lab} = 200$ MeV. We show in Fig. 5 only the calculations with combinations (a) and (e), because combination (a) can reproduce the fission cross sections in the reaction $^{32}S + ^{100}Mo$ [23], whereas combination (e) gives rise to systematically lower values for the σ_{FF} compared to the other combinations.

At beam energy above 200 MeV, calculations and experimental data show different trends. The SM predicts a suppression of the fission cross section, whereas the experimental data show an increase [35,67]. A possible explanation of the

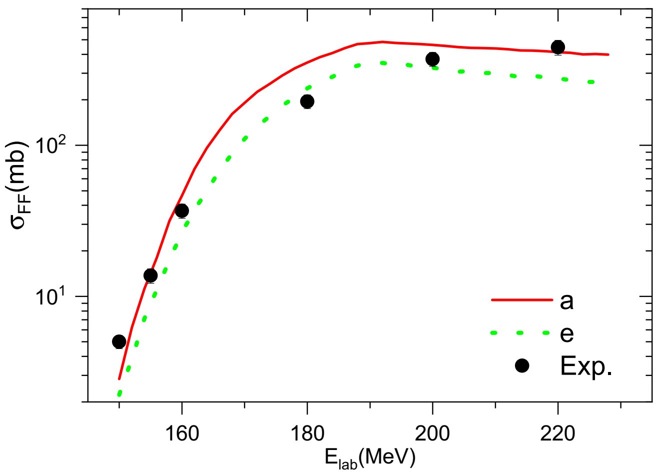

FIG. 5. Fission excitation function for the reaction $^{32}S + ^{126}Te$ (dots) (taken from Ref. [35]) compared with two PACE2_N11 calculations: (a) combination [solid red (gray) line] and (e) combination (dashed green line). For more details, see the text and Table II.

experimental trend can be the contribution of fast fission to σ_{FF}, which is not experimentally distinguishable from the fusion-fission one [11]. The non-negligible amount of fast fission affects also the extraction of prescission light particle multiplicities used to estimate the fission delay time (for a detailed discussion, see Ref. [33]). At energies above 200 MeV, the maximum angular momentum l_{max} is larger than $\approx 80\hbar$, namely, larger than critical angular momentum l_{crit} from the Bass model [68]. For the partial waves where $l > l_{crit}$ the fission barrier vanishes, according to the rotating-liquid-drop model [62], and the fast-fission dominates. This interpretation of a transition from fusion-fission to faster reactions at energy around 10 MeV/A is supported by experimental findings. In fact, the "extra-push" model was adopted to reproduce the fission cross sections in this energy region [67]. On these grounds, our choice of 180-MeV beam energy is well suited for the study of CN fission dynamics, with l_{max} smaller than the critical angular momentum and the fission cross section still relatively large.

In conclusion, the fission cross section can be reproduced with sufficient accuracy by the PACE2_N11 code with combinations from (a) to (f). It must be remarked that this means that the fission excitation function does not show an appreciable sensitivity to the set of parameters used for the calculations. In other words, it is not a good observable to discriminate among several models or parameter choices. On the contrary, strong constraints are imposed, as shown in the next, by the comparison with other observables, i.e., the charged particles in the ER and prescission channels.

B. Light particle multiplicities

The extracted LCP evaporation and prescission multiplicities are reported in Table III together with the fission cross section and the prescission neutron multiplicity from Refs. [35,67].

TABLE III. Light particle multiplicities in the ER and prescission channels for the $^{32}S + ^{126}Te$ reaction.

	ER			Prescission		
	M_n	M_p	M_α	M_n	M_p	M_α
Exp.		0.375 (0.075)	0.234 (0.047)	1.7[a] (0.5)	0.034 (0.007)	0.020 (0.004)
a	6.25	0.195	0.315	1.33	0.0072	0.0028
b	5.90	0.297	0.781	1.08	0.0095	0.0035
c	5.95	0.160	0.469	1.12	0.0049	0.0030
d	5.23	0.303	0.631	1.44	0.0320	0.0200
e	4.71	0.306	1.432	0.94	0.0255	0.0207
f	6.67	0.372	0.290	2.08	0.0305	0.0163

[a]From Ref. [34].

At first, we notice that the experimental proton multiplicity in the ER channel ($M_p(ER)$) is always underestimated, except for the (d) and (e) combinations that reproduce the data. α-particle multiplicity in the ER channel ($M_\alpha(ER)$) is instead always overestimated, up to a factor 6 for the (e) combination. This result is relevant because if this overestimation is replicated in the calculation of the prescission multiplicity, an unreliable estimate of the fission delay and nuclear viscosity parameters will result.

The values of $M_\alpha(ER)$ can be reduced by adopting a smaller value of the α-particle curvature in TC, as, for instance, in combination (f). Although all particle multiplicities are reproduced, combination (f) does not reproduce the α-particle spectrum as shown in Fig. 7, due to a significant cut at low energies. Furthermore, it produces proton-ER angular distribution amplitudes much larger than the experimental ones as discussed in the next subsection and shown in Fig. 8.

To shed some light on the controversial above results, more exclusive observables have been considered to make us confident about the correct evaluation of the CN decay where the particle emissions compete with fission. Finally, we remark that the maximum angular momentum $l_{\max}$, as fixed from the measured fission cross section, does not affect particle multiplicity calculations in the evaporation channel, but it does in the prescission channel. Hence, the results above are not related to the maximum of angular momentum chosen.

C. LCP-ER spectra

Figures 6 and 7 show two representative examples of proton and α-particle energy spectra measured in coincidence with ERs compared with the results of the simulations. All the spectra are normalized to the maximum. In the computed spectra, telescope and PPAC efficiency are taken into account.

It is quite evident that the calculated spectra are very sensitive to the simulation parameters in Table II. The combination (f), which simultaneously reproduces evaporative and prescission particle multiplicities, produces an α-particle spectrum that is very different from the experimental one, in particular, both at low and high energies. This is mainly due to the value of the barrier curvature for α particles $\hbar\omega_\alpha = 0.5$ MeV. For protons, where we used a curvature $\hbar\omega_p = 4$ MeV, we notice

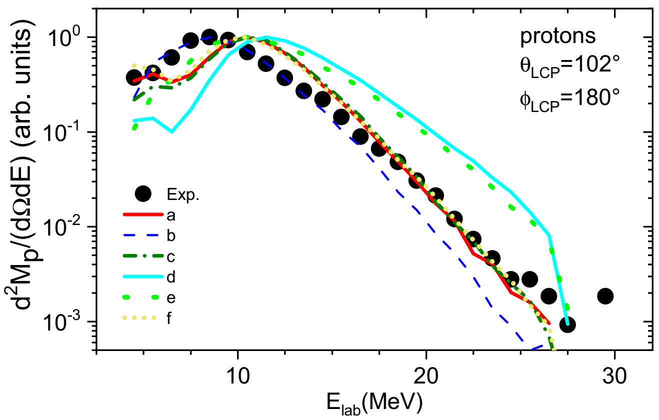

FIG. 6. Proton energy spectrum measured in coincidence with ER in the PPAC (dots) and the simulations (lines) obtained with the parameter combinations in Table II. The model combinations correspond to lines: (a) solid red (gray), (b) dashed blue, (c) dash-dotted olive, (d) solid cyan (light gray), (e) dotted green, and (f) short-dotted yellow. All the spectra are normalized to the maximum. For more details, see the text.

that combination (f) produces a proton spectrum very similar to those obtained using the combinations (a), (c), and (d) adopting also FS-TC. As a side note, we point out that, for reactions similar to the one studied here, experiments and theory indicate neutrons as the most probable ejectiles in CN-decay cascades [69,70]. In this respect, to reproduce the multiplicity ratios among the different particles in the prescission channel as well as in the evaporative one, an unusually large value of TC neutron curvature $\hbar\omega_n = 9.5$ MeV is necessary [71]. Consequently, we expect that also the neutron spectra will be affected, but we cannot check this point because information on this observable are not available.

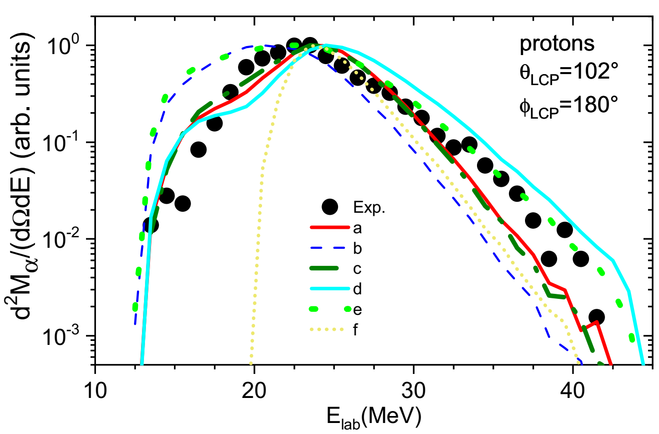

FIG. 7. α-particle energy spectrum measured in coincidence with ER in the PPAC (dots) and the simulations (lines) obtained with the parameter combinations in Table II. The model combinations correspond to lines: (a) solid red (gray), (b) dashed blue, (c) dash-dotted olive, (d) solid cyan (light gray), (e) dotted green, and (f) short-dotted yellow. All the spectra are normalized to the maximum. For more details, see the text.

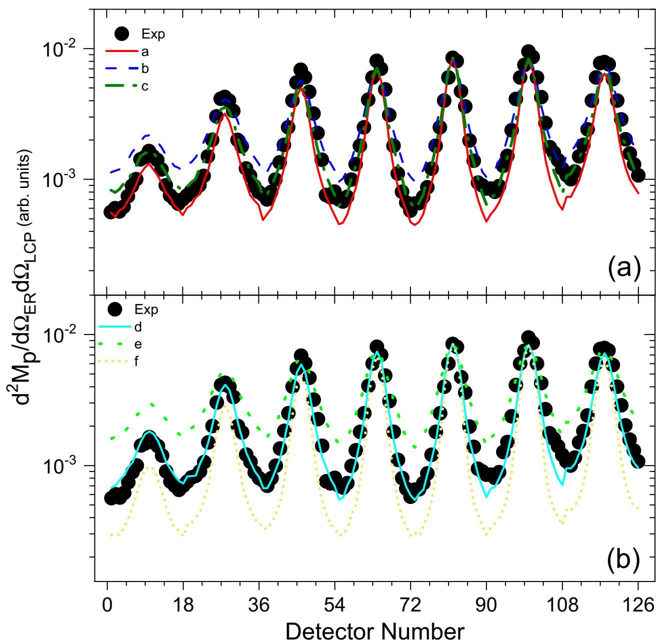

FIG. 8. Proton energy-integrated differential multiplicities measured with the Ball telescopes in correlation with ERs detected with the PPAC system (dots) and the simulations (lines) obtained with the parameter combinations in Table II. In panel (a), the solid red (gray), dashed blue and dash-dotted olive lines correspond to the (a), (b), and (c) combinations, respectively. In panel (b), the solid cyan (light gray), dotted green, and short-dotted yellow lines correspond to the (d), (e), and (f) combinations, respectively. In both panels, experimental (Exp) data are the same as in Fig. 3. Simulated data have been normalized to the maximum of the experimental data. See the text for more details.

From Fig. 6, we can deduce that combination (b), which employs OM-TC, provides the best agreement with the measured spectrum. The use of level density parameter equal to $a = A/6$ is important to well reproduce the high-energy side of all the spectra. Negligible are the differences obtained by assuming the emitting nucleus as a rigid sphere with $r_0 = 1.21$ fm or by a LDM deformation combinations (a) and (c), respectively.

Unlike protons, the best reproduction of the α-energy spectra has been achieved with combinations (a) and (c), both employing the FS-TC from Ref. [66]. However, for α particles, as well as for the protons, the differences among emitting nuclei described as rigid spheres with $r_0 = 1.21$ fm or with LDM deformations are very small. The level density parameters equal to $a = A/6$ and $A/12$ similarly reproduce the high-energy side; $a = A/6$ provides a better agreement because the maximum of the spectrum is closer to the experimental one. The FS-TC with curvature values of (a) and (c) combinations largely improve the reproduction of the α spectra, which is the opposite of what happens in case of protons.

The analysis of both LCP energy spectra seems to exclude the presence of a significant deformation of the CN in the fusion evaporation channel and indicates that the level density parameter $a = A/6$ is the most appropriate value. Unfortunately, none of the two TC parameters adopted reproduces simultaneously the low-energy sides of proton and α-particle energy spectra. To smooth out the observed discrepancies, different solutions have been considered. For instance, to shift proton spectra for the (a) and (c) combinations to lower energy, larger deformations of the CN can be adopted. However, α-particle spectra shift more than proton spectra for the same CN deformation. Consequently, a larger deformation will shift the α spectra at much lower energy and the experimental spectra will be not reproduced anymore. It must be pointed out that the disagreement observed with combination (b) for the α-particle spectra based on the use of OM-TC has been observed also for a previously studied intermediate-mass system, produced under similar experimental conditions [31], and that the observed limits of the SM in reproducing the energy spectra have been reported also by other authors in different mass and energy regions [72–74]. Moreover, it is worth noting that, in our opinion, the relatively small discrepancies observed with most of the combinations is indicative of a some missing physical ingredient, which is likely to be connected with the dynamics of the decay process [57].

D. LCP-ER angular distributions

Two additional observables that serve as a further source of information on the most appropriate SM parameter combination are the energy-integrated particle differential multiplicities in the evaporation channel. Figures 8 and 9 shows the differential multiplicity in comparison with the PACE2_N11 simulations. The simulated distributions were obtained by filtering the PACE2_N11 event output file through the 8πLP and PPAC system response functions. Then, the simulated distributions have been normalized to the maximum of the experimental data to better highlight the differences in shapes. The shift produced by the normalization is related to the ER channel multiplicities discussed in a previous section, whereas the maximum-minimum amplitudes of the oscillating curves depend on the kinematics and angular-momentum correlations as discussed in Sec. III A.

The experimental proton distribution (Fig. 8) is similarly well reproduced by combinations (a), (c), and (d). We notice that the use of a larger level density parameter and a slightly smaller deformation in combination (a) produces a reduction of the amplitudes at the backward direction. Even if the proton curvature $\hbar\omega_p$ used in the combination (f) is the same of (a), (c), and (d), the amplitudes of the differential multiplicity predicted by combination (f) are definitely larger and strongly deviate from the experimental ones. The amplitudes obtained with the OM-TC of combinations (b) and (e) are much smaller than experimental ones. The disagreement between the predictions of the energy-integrated differential multiplicity with the combination (b) and the data are not observed in the proton energy spectra. These latter, in fact, are well reproduced at low- and high-energy sides. A possible explanation of this behavior can be related to the increase of α-particle multiplicities of the ER channel in combination (b), as shown in Table III. This increase of α-particle multiplicity implies a reduction of the mean angular mo-

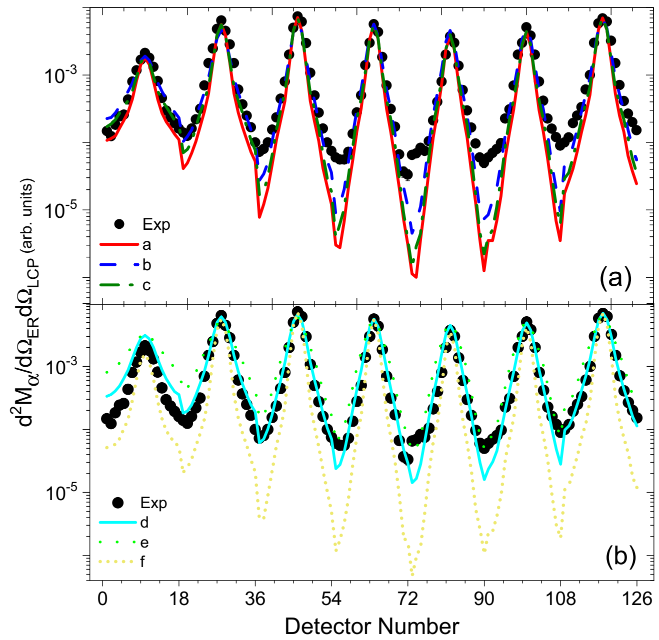

FIG. 9. α-particle energy-integrated differential multiplicities measured with the Ball telescopes in correlation with ERs detected with the PPAC system (dots) and the simulations (lines) obtained with the parameter combinations in Table II. In panel (a), the solid red (gray), dashed blue, and dash-dotted olive lines correspond to the (a), (b), and (c) combinations, respectively. In panel (b), the solid cyan (light gray), dotted green, and short-dotted yellow lines correspond to the (d), (e), and (f) combinations, respectively. In both panels, experimental (Exp) data are the same as in Fig. 3. Simulated data have been normalized to the maximum of the experimental data. See the text for more details.

mentum of excited nuclei emitting protons and consequently the amplitudes of the proton energy-integrated DM will be smaller.

Concerning α-particle differential multiplicity (Fig. 9), the worse case is obtained by the combination (f). In contrast, the best case is given by combination (e). Each of three parameters in combination (e) differing from the (a) one (smaller value of "little a," slightly larger nuclear deformations and OM-TC) produces a reduction of the amplitudes and consequently a better agreement with the experimental data. However, combination (e) does not reproduce $M_\alpha(ER)$ and α-particle energy spectra.

As a general trend for the α particles, we observe that the amplitudes in the differential multiplicity seem to be correlated with the α-particle multiplicities and not with the energy spectra. In fact, the smaller amplitudes are observed with the combination (e), the one that produces the higher $M_\alpha(ER)$, namely, with cascades where the mean angular momentum carried away by the α particles is smaller.

E. Overview of the comparison with the SM

As summarized in Table IV, the combination (f) well reproduces the particle multiplicities in both prescission and evaporation channels. Consequently, one could conclude that the SM gives a correct picture of the fission process and there is no need for a fission delay time. However, considering two additional observables, energy spectra and differential multiplicities, this conclusion is not supported anymore. In fact, a poor agreement is obtained in the comparisons of energy-integrated DMs and LCP energy spectra. We can name energy spectra and energy-integrated differential multiplicities exclusive observables. If we exclude them, combination (f) is the preferred choice of ingredients and parameters that reproduces all the multiplicity data.

Combinations (a) and (c), by reproducing the exclusive observables and underestimating the LCP prescission multiplicities, indicate the necessity of including a fission delay. All other the remaining combinations, which very badly reproduce at least one of the exclusive observables, can be disregarded.

This result is in line with those obtained for the system $^{32}S + ^{100}Mo$ [23,57], studied in similar experimental conditions. However, we have to notice that in this work the comparison has been extended also to the prescission neutron multiplicity, largely used in pioneering works, e.g., Refs. [18,34,75], and still in recent ones, e.g., Refs. [29,30], to estimate the fission delay and to determine the nuclear properties characterizing the fission process. This observable, although providing a further constraint to the model, is less sensitive compared to the exclusive observables measured

TABLE IV. Summary of the comparison of the model predictions with the experimental observables of the reaction $^{32}S + ^{126}Te$. The good and fair agreement of experimental values is indicated with $\surd$. The underestimated (overestimated) values of the multiplicities are indicated with U (O). The poor agreement of the LCP energy spectra and DM distributions in the ER channel are indicated with ✗.

	Multiplicities					E spectra		DMs	
	$M_p(ER)$	$M_\alpha(ER)$	$M_n(pre)$	$M_p(pre)$	$M_\alpha(pre)$	p	α	p	α
a	U	O	$\surd$	U	U	$\surd$	$\surd$	$\surd$	$\surd$
b	$\surd$	O	$\surd$	U	U	$\surd$	✗	✗	$\surd$
c	U	O	$\surd$	U	U	$\surd$	$\surd$	$\surd$	$\surd$
d	$\surd$	O	$\surd$	$\surd$	$\surd$	✗	$\surd$	$\surd$	$\surd$
e	$\surd$	O	U	$\surd$	$\surd$	✗	✗	✗	$\surd$
f	$\surd$	$\surd$	$\surd$	$\surd$	$\surd$	$\surd$	✗	✗	✗

in this work. However, neutron energy spectra in the ER channel would provide a very important additional constraint considering the competition with the emission of LCPs.

VI. DISCUSSION AND CONCLUSIONS

In this work, a severe test of the SM has been carried out by considering a wide set of observables measured along with existing experimental data. Extensive calculations have been carried out with the statistical model code PACE2_N11, and the predictions with the six most significant SM parameter combinations have been presented.

All the six combinations reasonably well reproduce the fission cross section measured with ^{32}S beam at 180 MeV on ^{126}Te target and its excitation function at energies around the Coulomb barrier. Although combination (f) ($a = A/7$, moment of inertia calculated by assuming compound nuclei as a rigid spheres with radius parameter $r_0 = 1.65$ fm and FS-TC with $\hbar\omega = 9.5, 4.0$, and 0.5 MeV for neutrons, protons, and α particles, respectively) allows us to reproduce all the multiplicities in the fusion-evaporation and prescission channels, it fails in modeling the evaporation channel exclusive observables: energy spectra and energy-integrated differential multiplicities of light-charged particles. The comparison with calculations has shown the high sensitivity of these latter observables to the parameters considered. This is relevant because by analyzing LCPs energy and angular distributions it is possible to get indications on the properties of the emitting nuclei such as, for instance, the nuclear deformation (that influences the yrast line and the transmission coefficients) and temperature (that influences the level density).

In summary, we find the following:

(1) The FS-TC (with curvatures 4, 4, and 3.5 MeV) seems to be more appropriate than OM-TC; i.e., FS-TC well reproduce the α-particle spectra and is in small disagreement with the proton energy spectra.

(2) The YL prescription describing the nuclear shapes as a rigid spheres with $r_0 = 1.21$ fm provides better LCP multiplicities than LDM, while the exclusive observables distribution are very similar.

(3) $a = A/6$ better reproduces all observables, except for the α-particle energy-integrated differential multiplicity distribution.

Hence, the exclusive observables in the evaporation channel, as well as fission cross section, are better reproduced with a level density parameter $a = A/6$, FS-TC (with curvatures 4, 4, 3.5 MeV) and rigid sphere YL with $r_0 = 1.21$ fm, namely, combination (a). Furthermore, combination (a) reproduces within a factor of less than 2 the evaporative proton and α-particle multiplicities. A discrepancy is still observed for the α-particle energy-integrated differential multiplicity distribution. However, it should be mentioned that this observable can be better reproduced if the amount of α particles emitted at higher angular momenta is reduced. Such effect can be obtained by modifying the evaporation-fission competition and we expect to get it by adopting a dynamical model that more realistically describes the excited nuclei decay processes.

We have to notice that, on one side, combination (a) underestimates the prescission multiplicities and, consequently, indicates a fission delay time larger than zero according to the well-known neutron clock method [18]. On the other, combination (f) reproduces all the multiplicities without the need for a fission delay. This conclusion is the only apparently controversial result. In fact, only the combination (a) can be considered reliable because it reproduces the exclusive observables in the ER channel. These results confirm the previous findings concerning the fission dynamics study in intermediate fissility systems [23,31,32] and the relevant role played by the ER channel in order to progress in the present understanding of fission dynamics.

In conclusion, the comprehensive analysis presented here seems to indicate the need to account for a fission delay time, while no evidence has been observed for deformations larger than those predicted by LDM. In addition, this work explored the most appropriate range for SM parameters in the mass and energy regions explored. Therefore, this analysis is important to get a general view on the fission process by reducing the ranges of variability for the SM parameters and corroborates subsequent analysis with more realistic models, e.g., dynamical models. By following the time evolution of the CN through the de-excitation processes, dynamical models are expected to shed light on the fission process to answer open questions concerning the nature and strength of the nuclear viscosity and the fission time distribution.

ACKNOWLEDGMENT

The authors wish to thank the staff at LNL for the excellent technical support in carrying out the experiment.

[1] L. Meitner and O. R. Frisch, Nature (London) **143**, 239 (1939).
[2] O. Hahn and F. Strassmann, Naturwiss **27**, 11 (1939).
[3] K.-H. Schmidt and B. Jurado, Rep. Prog. Phys. **81**, 106301 (2018).
[4] A. N. Andreyev, K. Nishio, and K. H. Schmidt, Rep. Prog. Phys. **81**, 016301 (2018).
[5] J. Khuyagbaatar, D. J. Hinde, I. P. Carter, M. Dasgupta, C. E. Düllmann, M. Evers, D. H. Luong, R. du Rietz, A. Wakhle, E. Williams, and A. Yakushev, Phys. Rev. C **91**, 054608 (2015).
[6] E. M. Kozulin, E. Vardaci, I. M. Harca, C. Schmitt, I. M. Itkis, G. N. Knyazheva, K. Novikov, A. Bogachev, S. Dmitriev, T. Loktev, F. Azaiez, I. Matea, D. Verney, A. Gottardo, O. Dorvaux, J. Piot, G. Chubarian, W. Trzaska, F. Hanappe, C. Borcea, S. Calinescu, and C. Petrone, Eur. Phys. J. A **52**, 293 (2016).
[7] A. Saxena, D. Fabris, G. Prete, D. V. Shetty, G. Viesti, B. K. Nayak, D. C. Biswas, R. K. Choudhury, S. S. Kapoor, M. Barbui, E. Fioretto, M. Cinausero, M. Lunardon, S. Moretto, G. Nebbia, S. Pesente, A. M. Samant, A. Brondi, G. La Rana, R. Moro, E. Vardaci, A. Ordine, N. Gelli, and F. Lucarelli, Phys. Rev. C **65**, 064601 (2002).
[8] R. Léguillon, K. Nishio, K. Hirose, H. Makii, I. Nishinaka, R. Orlandi, K. Tsukada, J. Smallcombe, S. Chiba, Y. Aritomo, T. Ohtsuki, R. Tatsuzawa, N. Takaki, N. Tamura, S. Goto, I.

Tsekhanovich, C. M. Petrache, and A. N. Andreyev, Phys. Lett. B **761**, 125 (2016).

[9] J. L. Rodríguez-Sánchez, J. Benlliure, J. Taïeb, H. Alvarez-Pol, L. Audouin, Y. Ayyad, G. Bélier, G. Boutoux, E. Casarejos, A. Chatillon, D. Cortina-Gil, T. Gorbinet, A. Heinz, A. Kelić-Heil, B. Laurent, J. F. Martin, C. Paradela, E. Pellereau, B. Pietras, D. Ramos, C. Rodríguez-Tajes, D. M. Rossi, H. Simon, J. Vargas, and B. Voss, Phys. Rev. C **94**, 061601(R) (2016).

[10] M. G. Itkis, E. Vardaci, I. M. Itkis, G. N. Knyazheva, and E. M. Kozulin, Nucl. Phys. A **944**, 204 (2015).

[11] G. Fazio, G. Giardina, G. Mandaglio, R. Ruggeri, A. I. Muminov, A. K. Nasirov, Y. T. Oganessian, A. G. Popeko, R. N. Sagaidak, A. V. Yeremin, S. Hofmann, F. Hanappe, and C. Stodel, Phys. Rev. C **72**, 064614 (2005).

[12] B. B. Back, H. Esbensen, C. L. Jiang, and K. E. Rehm, Rev. Mod. Phys. **86**, 317 (2014).

[13] E. M. Kozulin, V. I. Zagrebaev, G. N. Knyazheva, I. M. Itkis, K. V. Novikov, M. G. Itkis, S. N. Dmitriev, I. M. Harca, A. E. Bondarchenko, A. V. Karpov, V. V. Saiko, and E. Vardaci, Phys. Rev. C **96**, 064621 (2017).

[14] E. Vardaci, M. G. Itkis, I. M. Itkis, G. Knyazheva, and E. M. Kozulin, J. Phys. G: Nucl. Part. Phys. **46**, 103002 (2019).

[15] S. Cohen, F. Plasil, and W. J. Swiatecki, Ann. Phys. **82**, 557 (1974).

[16] K. T. R. Davies, A. Sierk, and J. Nix, Phys. Rev. C **13**, 2385 (1976).

[17] A. J. Sierk and J. R. Nix, Phys. Rev. C **21**, 982 (1980).

[18] D. J. Hinde, D. Hilscher, H. Rossner, B. Gebauer, M. Lehmann, and M. Wilpert, Phys. Rev. C **45**, 1229 (1992).

[19] J. P. Lestone, Phys. Rev. Lett. **70**, 2245 (1993).

[20] H. Ikezoe, Y. Nagame, I. Nishinaka, Y. Sugiyama, Y. Tomita, K. Ideno, S. Hamada, N. Shikazono, A. Iwamoto, and T. Ohtsuki, Phys. Rev. C **49**, 968 (1994).

[21] I. Diószegi, N. P. Shaw, I. Mazumdar, A. Hatzikoutelis, and P. Paul, Phys. Rev. C **61**, 024613 (2000).

[22] T. Wada, Y. Abe, and N. Carjan, Phys. Rev. Lett. **70**, 3538 (1993).

[23] E. Vardaci, P. N. Nadtochy, A. Di Nitto, A. Brondi, G. La Rana, R. Moro, P. K. Rath, M. Ashaduzzaman, E. M. Kozulin, G. N. Knyazheva *et al.*, Phys. Rev. C **92**, 034610 (2015).

[24] D. Hilscher and H. Rossner, Ann. Phys. (Fr.) **17**, 471 (1992).

[25] P. Fröbrich and I. Gontchar, Phys. Rep. **292**, 131 (1998).

[26] D. Jacquet and M. Morjean, Prog. Part. Nucl. Phys. **63**, 155 (2009).

[27] J. P. Lestone, J. R. Leigh, J. O. Newton, D. J. Hinde, J. X. Wei, J. X. Chen, S. Elfstrom, and D. G. Popescu, Phys. Rev. Lett. **67**, 1078 (1991).

[28] N. P. Shaw, I. Diószegi, I. Mazumdar, A. Buda, C. R. Morton, J. Velkovska, J. R. Beene, D. W. Stracener, R. L. Varner, M. Thoennessen, and P. Paul, Phys. Rev. C **61**, 044612 (2000).

[29] K. Kapoor, S. Verma, P. Sharma, R. Mahajan, N. Kaur, G. Kaur, B. R. Behera, K. P. Singh, A. Kumar, H. Singh, R. Dubey, N. Saneesh, A. Jhingan, P. Sugathan, G. Mohanto, B. K. Nayak, A. Saxena, H. P. Sharma, S. K. Chamoli, I. Mukul, and V. Singh, Phys. Rev. C **96**, 054605 (2017).

[30] K. Kapoor, N. Bansal, C. Sharma, S. Verma, K. Rani, R. Mahajan, B. R. Behera, K. P. Singh, A. Kumar, H. Singh, R. Dubey, N. Saneesh, M. Kumar, A. Yadav, A. Jhingan, P. Sugathan, B. K. Nayak, A. Saxena, H. P. Sharma, and S. K. Chamoli, Phys. Rev. C **100**, 014620 (2019).

[31] A. Di Nitto, E. Vardaci, A. Brondi, G. La Rana, R. Moro, P. Nadtochy, M. Trotta, A. Ordine, A. Boiano, M. Cinausero, E. Fioretto, G. Prete, V. Rizzi, D. V. Shetty, M. Barbui, D. Fabris, M. Lunardon, G. Montagnoli, S. Moretto, G. Viesti, N. Gelli, F. Lucarelli, G. N. Knyazheva, and E. M. Kozulin, Eur. Phys. J. A **47**, 83 (2011).

[32] A. Di Nitto, E. Vardaci, G. La Rana, P. N. Nadtochy, and G. Prete, Nucl. Phys. A **971**, 21 (2018).

[33] G. La Rana, A. Brondi, R. Moro, E. Vardaci, A. Ordine, A. Boiano, M. A. Di Meo, A. Scherillo, D. Fabris, M. Lunardon, G. Nebbia, G. Viesti, M. Cinausero, E. Fioretto, G. Prete, N. Gelli, and F. Lucarelli, Eur. Phys. J. A **16**, 199 (2003).

[34] A. Gavron, A. Gayer, J. Boissevain, H. C. Britt, T. C. Awes, J. R. Beene, B. Cheynis, D. Drain, R. L. Ferguson, F. E. Obenshain, F. Plasil, G. R. Young, G. A. Petitt, and C. Butler, Phys. Rev. C **35**, 579 (1987).

[35] J. van der Plicht, H. C. Britt, M. M. Fowler, Z. Fraenkel, A. Gavron, J. B. Wilhelmy, F. Plasil, T. C. Awes, and G. R. Young, Phys. Rev. C **28**, 2022 (1983).

[36] P. N. Nadtochy, E. G. Ryabov, A. V. Cheredov, and G. D. Adeev, Eur. Phys. J. A **52**, 308 (2016).

[37] E. Vardaci, A. Di Nitto, A. Brondi, G. La Rana, R. Moro, P. N. Nadotchy, M. Trotta, A. Ordine, A. Boiano, M. Cinausero, E. Fioretto, G. Prete, V. Rizzi, D. Shetty, M. Barbui, D. Fabris, M. Lunardon, G. Montagnoli, S. Moretto, G. Viesti, N. Gelli, F. Lucarelli, G. N. Knyazheva, and E. M. Kozulin, Eur. Phys. J. A **43**, 127 (2010).

[38] E. Fioretto, M. Cinausero, M. Giacchini, M. Lollo, G. Prete, R. Burch, M. Caldogno, D. Fabris, M. Lunardon, G. Nebbia, G. Viesti, A. Boiano, A. Brondi, G. La Rana, R. Moro, A. Ordine, E. Vardaci, A. Zaghi, N. Gelli, and F. Lucarelli, IEEE Trans. Nucl. Sci. **44**, 1017 (1997).

[39] G. Prete, E. Fioretto, M. Cinausero, M. Giacchini, M. Lollo, D. Fabris, M. Lunardon, G. Nebbia, G. Viesti, M. Caldogno, A. Brondi, G. La Rana, R. Moro, E. Vardaci, A. Ordine, A. Zaghi, A. Boiano, P. Blasi, N. Gelli, and F. Lucarelli, Nuovo Cimento A **111**, 1089 (1998).

[40] A. Ordine, A. Boiano, E. Vardaci, A. Zaghi, and A. Brondi, IEEE Trans. Nucl. Sci. **45**, 873 (1998).

[41] M. Romoli, M. Di Pietro, E. Vardaci, A. De Francesco, M. Mazzocco, R. Bonetti, A. De Rosa, T. Glodariu, A. Guglielmetti, G. Inglima *et al.*, IEEE Trans. Nucl. Sci. **52**, 1860 (2005).

[42] D. Pierroutsakou, B. Martin, T. Glodariu, M. Mazzocco, R. Bonetti, A. D. Francesco, A. D. Rosa, F. Farinon, A. Guglielmetti, G. Inglima *et al.*, Eur. Phys. J. Spec. Top. **150**, 47 (2007).

[43] M. Mazzocco, C. Signorini, M. Romoli, R. Bonetti, A. D. Francesco, A. D. Rosa, M. D. Pietro, L. Fortunato, T. Glodariu, A. Guglielmetti *et al.*, Eur. Phys. J. Spec. Top. **150**, 37 (2007).

[44] C. Signorini, D. Pierroutsakou, B. Martin, M. Mazzocco, T. Glodariu, R. Bonetti, A. Guglielmetti, M. L. Commara, M. Romoli, M. Sandoli, E. Vardaci *et al.*, Eur. Phys. J. A **44**, 63 (2010).

[45] N. Patronis, A. Pakou, D. Pierroutsakou, A. M. Sánchez-Benítez, L. Acosta, N. Alamanos, A. Boiano, G. Inglima, D. Filipescu, T. Glodariu *et al.*, Phys. Rev. C **85**, 024609 (2012).

[46] E. Vardaci, VISM: A Computer Program for Nuclear Data Analysis, Annual Report, Carnegie Mellon University, Pittsburgh, USA, 1989.

[47] A. Di Nitto, E. Vardaci, A. Brondi, G. La Rana, M. Cinausero, N. Gelli, R. Moro, P. N. Nadtochy, G. Prete, and A. Vanzanella, Phys. Rev. C **93**, 044602 (2016).
[48] R. Moro, A. Brondi, N. Gelli, M. Barbui, A. Boiano, M. Cinausero, A. Di Nitto, D. Fabris, E. Fioretto, G. La Rana, F. Lucarelli, M. Lunardon, G. Montagnoli, A. Ordine, G. Prete, V. Rizzi, M. Trotta, and E. Vardaci, Eur. Phys. J. A **48**, 159 (2012).
[49] N. N. Ajitanand, R. Lacey, G. F. Peaslee, E. Duek, and J. M. Alexander, Nucl. Instrum. Meth. Phys. Res. A **243**, 111 (1986).
[50] V. E. Viola, K. Kwiatkowski, and M. Walker, Phys. Rev. C **31**, 1550 (1985).
[51] N. N. Ajitanand, G. La Rana, R. Lacey, D. J. Moses, L. C. Vaz, G. F. Peaslee, D. M. de Castro Rizzo, M. Kaplan, and J. M. Alexander, Phys. Rev. C **34**, 877 (1986).
[52] R. Lacey, N. N. Ajitanand, J. M. Alexander, D. M. de Castro Rizzo, G. F. Peaslee, L. C. Vaz, M. Kaplan, M. Kildir, G. La Rana, D. J. Moses, W. E. Parker, D. Logan, M. S. Zisman, P. DeYoung, and L. Kowalski, Phys. Rev. C **37**, 2540 (1988).
[53] W. E. Parker, M. Kaplan, D. J. Moses, J. M. Alexander, J. T. Boger, R. A. Lacey, and D. de Castro Rizzo, Nucl. Phys. A **568**, 633 (1994).
[54] R. Yanez, W. Loveland, L. Yao, J. S. Barrett, S. Zhu, B. B. Back, T. L. Khoo, M. Alcorta, and M. Albers, Phys. Rev. Lett. **112**, 152702 (2014).
[55] T. Banerjee, S. Nath, and S. Pal, Phys. Lett. B **776**, 163 (2018).
[56] A. Chatterjee, A. Navin, S. Kailas, P. Singh, D. C. Biswas, A. Karnik, and S. S. Kapoor, Phys. Rev. C **52**, 3167 (1995).
[57] E. Vardaci, A. Di Nitto, P. N. Nadtochy, and G. La Rana, J. Phys. G: Nucl. Part. Phys **46**, 115111 (2019).
[58] F. Pühlhofer, Nucl. Phys. A **280**, 267 (1977).
[59] W. Reisdorf, Z. Phys. A **300**, 227 (1981).
[60] D. Mahboub, C. Beck, B. Djerroud, R. M. Freeman, F. Haas, R. Nouicer, M. Rousseau, P. Papka, A. Sànchez iZafra, S. Cavallaro, E. De Filippo, G. Lanzanò, A. Pagano, M. Sperduto, E. Berthoumieux, R. Dayras, R. Legrain, E. Pollacco, and A. Hachem, Phys. Rev. C **69**, 034616 (2004).
[61] A. Gavron, Phys. Rev. C **21**, 230 (1980).
[62] A. J. Sierk, Phys. Rev. C **33**, 2039 (1986).
[63] J. Huizenga and G. Igo, Nucl. Phys. **29**, 462 (1962).
[64] F. G. Perey, Phys. Rev. **131**, 745 (1963).
[65] D. Wilmore and P. Hodgson, Nucl. Phys. **55**, 673 (1964).
[66] L. C. Vaz and J. M. Alexander, Z. Phys. A **318**, 231 (1984).
[67] A. Gavron, J. Boissevain, H. C. Britt, K. Eskola, P. Eskola, M. M. Fowler, H. Ohm, J. B. Wilhelmy, T. C. Awes, R. L. Ferguson, F. E. Obenshain, F. Plasil, G. R. Young, and S. Wald, Phys. Rev. C **30**, 1550 (1984).
[68] R. Bass, *Nuclear Reactions with Heavy Ions* (Springer-Verlag, Berlin, 1980).
[69] R. J. Charity, L. G. Sobotka, J. Cibor, K. Hagel, M. Murray, J. B. Natowitz, R. Wada, Y. El Masri, D. Fabris, G. Nebbia, G. Viesti, M. Cinausero, E. Fioretto, G. Prete, A. Wagner, and H. Xu, Phys. Rev. C **63**, 024611 (2001).
[70] P. N. Nadtochy, E. Vardaci, A. Di Nitto, A. Brondi, G. La Rana, R. Moro, M. Cinausero, G. Prete, N. Gelli, and F. Lucarelli, Phys. Lett. B **685**, 258 (2010).
[71] G. La Rana, R. Moro, A. Brondi, P. Cuzzocrea, A. D'Onofrio, E. Perillo, M. Romano, and F. Terrasi, Phys. Rev. C **40**, 2425 (1989).
[72] G. La Rana, D. J. Moses, W. E. Parker, M. Kaplan, D. Logan, R. Lacey, J. M. Alexander, and R. J. Welberry, Phys. Rev. C **35**, 373 (1987).
[73] G. La Rana, R. Moro, A. Brondi, P. Cuzzocrea, A. D'Onofrio, E. Perillo, M. Romano, F. Terrasi, E. Vardaci, and H. Dumont, Phys. Rev. C **37**, 1920 (1988).
[74] R. J. Charity, L. G. Sobotka, J. F. Dempsey, M. Devlin, S. Komarov, D. G. Sarantites, A. L. Caraley, R. T. deSouza, W. Loveland, D. Peterson, B. B. Back, C. N. Davids, and D. Seweryniak, Phys. Rev. C **67**, 044611 (2003).
[75] P. Paul and M. Thoennesen, Annu. Rev. Nucl. Part. Sci. **44**, 65 (1994), and references therein.